High-precision diode-laser-based temperature measurement for air refractive index compensation

Tuomas Hieta,[1,2] Mikko Merimaa,[1,*] Markku Vainio,[1,3] Jeremias Seppä,[1] and Antti Lassila[1]

[1]Centre for Metrology and Accreditation (MIKES), Tekniikantie 1, Espoo 02151, Finland

[2]Metrology Research Institute, Aalto University, Otakaari 5 A, Espoo 02150, Finland

[3]Laboratory of Physical Chemistry, Department of Chemistry, A. I. Virtasen aukio 1, University of Helsinki, Helsinki 00014, Finland

*Corresponding author: mikko.merimaa@mikes.fi

Received 2 May 2011; revised 9 September 2011; accepted 16 September 2011; posted 20 September 2011 (Doc. ID 146931); published 27 October 2011

We present a laser-based system to measure the refractive index of air over a long path length. In optical distance measurements, it is essential to know the refractive index of air with high accuracy. Commonly, the refractive index of air is calculated from the properties of the ambient air using either Ciddor or Edlén equations, where the dominant uncertainty component is in most cases the air temperature. The method developed in this work utilizes direct absorption spectroscopy of oxygen to measure the average temperature of air and of water vapor to measure relative humidity. The method allows measurement of temperature and humidity over the same beam path as in optical distance measurement, providing spatially well-matching data. Indoor and outdoor measurements demonstrate the effectiveness of the method. In particular, we demonstrate an effective compensation of the refractive index of air in an interferometric length measurement at a time-variant and spatially nonhomogeneous temperature over a long time period. Further, we were able to demonstrate 7 mK RMS noise over a 67 m path length using a 120 s sample time. To our knowledge, this is the best temperature precision reported for a spectroscopic temperature measurement.

OCIS codes: 120.0120, 140.0140, 120.6780, 120.3180, 140.2020.

1. Introduction

The refractive index of a medium, usually air, must be known accurately in optical length measurements, because the length scale is derived from the speed of light. The most accurate method for determination of the refractive index n is an optical refractometer. Optical refractometers determine n by measuring the wavelength difference in vacuum and in ambient air [1,2]. However, refractometers measure the refractive index over a short fixed beam path and usually require a laboratory environment. Thus, parameter-based Edlen and Ciddor equations are conventionally used and can reach an uncertainty in the 10^{-8} range [2–4]. Parameters affecting the refractive index of air include temperature, pressure, water vapor concentration, and CO_2 concentration. Sensitivity of the refractive index of air at 633 nm under standard ambient conditions is given in Table 1 for these parameters. Ambient pressure is generally homogeneous even over a long path length, and it is not usually the most dominant source of uncertainty [5]. Standard uncertainty of the order of 5 Pa is readily achievable. Also CO_2 concentration can be considered to be homogeneous and stable both in indoor and outdoor environments. Sensors capable of measuring the CO_2 concentration in the parts per million

0003-6935/11/315990-09$15.00/0

Table 1. Variation in Temperature, Pressure, Relative Humidity, and CO_2 Concentration That Will Result in 10^{-7} Increase in the Refractive Index of Air Based on the Modified Edlén Formula [1] Using a Wavelength of 633 nm

Parameter	Temperature	Pressure	Relative Humidity	CO_2 Concentration
Nominal Value	20 C	101.3 kPa	50%	400 ppm
Difference	−0.11 C	+0.037 kPa	−11.6%	+700 ppm

(ppm) range are commercially available, and can be used when large variations are expected or high accuracy is needed. Water vapor concentration at standard conditions has a relatively small effect on the refractive index of air, but, for example, at 35 °C, which is not uncommon outdoors or in an industrial environment, a measurement uncertainty of less than 5% is necessary to reach refractive index compensation below 10^{-7}.

In most cases, the uncertainty in the air temperature measurement dominates the combined uncertainty of refractive index determination. Under excellent laboratory conditions [6], air temperature can be measured to a high degree of accuracy using an ensemble of conventional temperature sensors. When performing optical distance measurements over tens of meters under industrial or outdoor conditions, air temperature measurement at a level required to reach, e.g., 10^{-7} uncertainty in distance is difficult or impossible, as the accuracy of temperature-sensor-based setups is deteriorated due to temporal and spatial air temperature variations. Thus, a method allowing fast measurement of air temperature over the path used in the optical distance measurement is desired. For a range of a few meters, an acoustic method based on the speed of sound measurement of an ultrasound burst signal can be used [7]. In this work, we have studied refractive index compensation using spectroscopy-based laser thermometry that allows temperature measurements over long path lengths.

Laser spectroscopy has been extensively used for noninvasive temperature sensing in gases [8–20]. Much of the research has been focused on combustion applications at elevated temperatures. Wavelength modulation absorption spectroscopy (WMAS) has recently received the most attention [10–15], but direct absorption spectroscopy measurements have also proven successful [16–19]. WMAS is generally preferred over direct absorption because only the peak values are required for thermometry.

We demonstrate that our system is capable of effectively compensating for the refractive index of air, even when temperature gradients are induced along the measurement path and conventional temperature sensors fail. The developed measurement system is capable of determining relative humidity and temperature over a long distance and along the interferometer beam path, resulting in an uncertainty smaller than 10^{-7} in the refractive index of air within a temperature range extending from 16 °C to 25 °C.

2. Experimental Setup

In a previous work [19] we presented a proof-of-principle on spectroscopic air temperature measurement with a RMS noise of 22 mK, which corresponds to an $\sim 2 \cdot 10^{-8}$ RMS noise in the refractive index of air. Since then, the setup and data processing has been refined and an arrangement for relative humidity measurement was combined with our system for more complete refractive index of air compensation. The humidity measurement utilizes the same modulated and normalized absorption technique as the temperature measurement setup, but instead of measuring the ratio of two absorption peaks, only one water transition and baseline determination are required for determining the number density of water. A detailed description of the humidity measurement configuration and results is given in [21].

The combined measurement configuration is schematically shown in Fig. 1. Oxygen spectroscopy is done using two selected distributed feedback (DFB) lasers (Eagleyard EYP-DFB-0760) operating around 762 nm and having integrated temperature controls. Two selected DFB lasers (Sarnoff SAR-815-DFB) near 816 nm are used for water spectroscopy. Each laser has its own shutter and attenuator to optimize

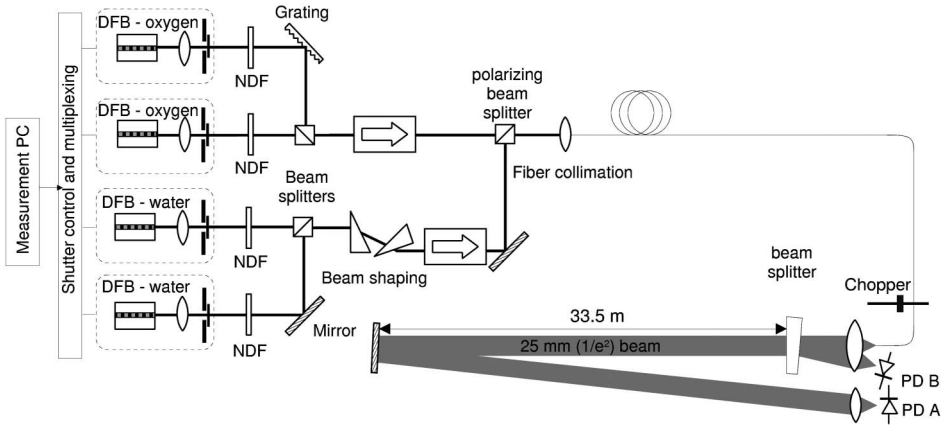

Fig. 1. Schematic temperature measurement setup using a 67 m path length. Two water spectroscopy lasers are not in use.

the dynamic range of detection. During measurements, the spectral purity of one of the lasers used for oxygen spectroscopy was degraded, although the performance remained within the manufacturer's specification. It is known that diode laser output characteristics change over time, which unfortunately had a significant impact on our system's performance, as broadband emission outside the main mode causes errors in signal normalization. The grating was included in the setup to suppress spurious emission with good results. At the very end of our measurement period, which lasted around six months, the spectral purity of the other oxygen laser also had to be improved using a grating.

A polarizing beam splitter is used to combine light from the lasers for oxygen and water spectroscopy. Beam shaping with a prism pair is used for the SAR-815-DFB lasers to achieve improved fiber coupling efficiency. Low-loss single-mode fiber is used between the fiber coupling lens and measurement head. A high-quality aspheric lens (Asphericon 50-100 LPX-U) collimates the beam coming out from the fiber end. To reach a low sensitivity to polarization rotation in the fiber, a metallic beam splitter nearly perpendicular to the beam is placed close to the collimation lens to sample part of the output beam to photodiode B (PD B), while the other part of the beam is used for spectroscopy and detected with photodiode A (PD A). The normalization scheme used in the setup effectively cancels small drifts in the laser output power, interferences caused by the optics before the measurement head, varying fiber coupling efficiency, and rotation in the light polarization. A double-pass scheme using a dielectric mirror is used for practical reasons. It enables the use of the same measurement head for both transmitting and receiving. The double-pass scheme also compensates reasonably well the effect of absorption-induced power loss that leads to a weighted average. In comparison, in a simple single-pass scheme, the signal intensity can be much higher in the transmitting end than in the receiving end, leading to a weighted average that erroneously gives higher weight closer to the transmitting end. A mechanical chopper and a lock-in amplifier (SR-830) are used for detection of signals A and B at 1.6 kHz. An active control of the beam direction, based on piezoelectric transducers and a position sensitive detector, which is not shown in Fig. 1, close to PD A centers the reflected beam to the detector lens. Active control was found to be important both in outdoor and indoor environments. It compensates the thermal lensing effects caused by nonhomogeneous temperature distributions that otherwise lead to a random clipping of the beam edges. The measurement head electronics were connected to the measurement computer using an Ethernet for improved flexibility.

3. Theory and Line Selection

The widely used HITRAN [22–25] database was used to obtain molecular parameters for calculations and to simulate the transmission spectrum of air. Therefore, notations adopted from HITRAN are used to describe the molecular transmission properties presented in this section. The Beer–Lambert law is the fundamental equation that relates the light intensity I after a sample to the dimensionless optical thickness for a single transition $\tau_{\eta\eta'}$, according to

$$I = I_0 e^{-\tau_{\eta\eta'}}, \tag{1}$$

where I_0 is the intensity before the sample. For a single transition at frequency $\nu_{\eta\eta'}$ between lower and upper states η and η', the optical thickness for a gas at pressure p, temperature T, and at frequency ν, is calculated as

$$\tau_{\eta\eta'}(\nu, T, p) = uS_{\eta\eta'}(T) f(\nu, \nu_{\eta\eta'}, T, p) = uk_{\eta\eta'}(\nu, T, p), \tag{2}$$

where $S_{\eta\eta'}$ is the line intensity, f is the normalized line shape function, and u is the number density of absorbing molecules per unit path length. The monochromatic absorption coefficient $k_{\eta\eta'}$ is the product of a normalized line shape function and the line intensity. The line shape function, which is characterized by line half-width γ, is in general affected by both Doppler and pressure broadening. Doppler broadening is characterized by a Gaussian line profile and pressure broadening by a Lorentzian line profile. The actual line profile is obtained as a convolution of these two, which results into a Voigt line shape. In the lower atmosphere, the oxygen line shape function is dominated by the Lorentzian profile. We have used an approximate solution for the Voigt line shape [26] in the spectral simulations and a convoluted solution in all the calculations in this paper.

The temperature-dependent line intensity $S_{\eta\eta'}(T)$ can be calculated from the tabulated line intensity at reference temperature T_{ref} of 296 K using

$$S_{\eta\eta'}(T) = S_{\eta\eta'}(T_{\mathrm{ref}}) \frac{Q(T_{\mathrm{ref}})}{Q(T)} \exp\left[-\frac{hcE_\eta}{k}\left(\frac{1}{T} - \frac{1}{T_{\mathrm{ref}}}\right)\right] \times \left[\frac{1 - \exp(-hc\nu_{\eta\eta'}/kT)}{1 - \exp(-hc\nu_{\eta\eta'}/kT_{\mathrm{ref}})}\right], \tag{3}$$

where $Q(T)$ is the total internal partition sum, E_η is the lower state energy, h is the Planck constant, k is the Boltzmann constant (not to be confused with the monochromatic absorption coefficient $k_{\eta\eta'}$), and c is the speed of light. The third term in Eq. (3) accounts for the ratio of Boltzmann populations between temperature T and the reference temperature T_{ref}. The last term accounts for the effects of stimulated emission, which is negligible at the visible wavelength region.

The temperature of air can be spectroscopically determined from the ratio of two oxygen transitions that have different lower state energies [8]. The ratio of the line intensities of the two transitions is given by

$$R = \frac{S_1(T)}{S_2(T)} = \frac{S_1(T_{\mathrm{ref}})}{S_2(T_{\mathrm{ref}})} \exp\left[-\frac{hc\Delta E}{k}\left(\frac{1}{T} - \frac{1}{T_{\mathrm{ref}}}\right)\right]$$
$$= R_0 \exp\left[-\frac{hc\Delta E}{k}\left(\frac{1}{T} - \frac{1}{T_{\mathrm{ref}}}\right)\right], \quad (4)$$

where ΔE is the difference in their rotational energies and R_0 is the ratio of S_1/S_2 at reference temperature. The oxygen transitions at $\lambda_1 = 761,715\,\mathrm{nm}$ $\lambda_2 = 759,831\,\mathrm{nm}$ were used in the measurements reported here and are marked with subindices 1 and 2, respectively. For absolute determination of the temperature, the line intensity ratio at the reference temperature must be known accurately. For example, a 10^{-3} error in the line intensity ratio will change the temperature by ~120 mK when using transitions 1 and 2 at standard temperature and pressure. Based on Eq. (4), the rotational energy difference must be large in order to achieve high temperature sensitivity. Our approach is to use two weak transitions of the oxygen A-band R-branch near 762 nm for thermometry. The oxygen A-band [27–29] has several weak transitions that are well separated and virtually interference free from other molecular transitions, making it well suited for thermometry over long path lengths. In addition, oxygen concentration can be assumed to be very stable over time both in indoor and outdoor environments compared to, for example, water, which is often used in laser thermometry. The relevant parameters obtained from the HITRAN database [23–25] for the two chosen oxygen transitions are shown in Table 2. Hereafter, wavelength λ is used for describing the transition positions. The temperature measurement should be, in principle, independent of the path length according to Eq. (4). In practice, clipping of the beam edges due to poor alignment of the optical components or measuring over long distances will degrade the performance. In addition, the beam collimation is slightly dependent on the wavelength, thus making it impossible to collimate the two laser beams simultaneously over long distances. This will lead to a lead to independent clipping of the beams.

The simulated spectral transmission over a 67 m path length using the standard 20.95% oxygen concentration was calculated using the HITRAN database values and is given in Fig. 2. Figure 2 also shows the calculated relative change in the transmission for 1 K change in temperature. The center of the R-branch of the A-band transition becomes highly saturated at distances beyond tens of meters and, therefore, is not suitable for long-distance high-accuracy thermometry. The transitions used in this work are marked in Fig. 2 together with the point of the baseline measurement. In theory, the absolute temperature could be determined using only the ratio of the line intensities at reference temperature and the rotational energy difference. Although the baseline is not theoretically necessary for thermometry, it can have major impact on the results if omitted [19]. The small absorbance due to the tails of the Voigt profile is hence taken into account in the baseline measurements.

Table 2. Parameters for the Oxygen Transitions Used in This Work at Reference Pressure of 1 atm and Temperature of 296 K (*n* Denotes the Temperature Coefficient of the Temperature-Dependent Linewidth)

$\nu_{\eta\eta'}$ (cm^{-1})	λ (nm)	$S_{\eta\eta'}(T_{\mathrm{ref}})$ (cm/molecule)	E_η (cm^{-1})	γ_{air} (cm^{-1})	n (1)
13128.27	761.715	3.583×10^{-24}	2.1	0.0563	0.71
13160.82	759.831	2.246×10^{-24}	544.5	0.0401	0.64

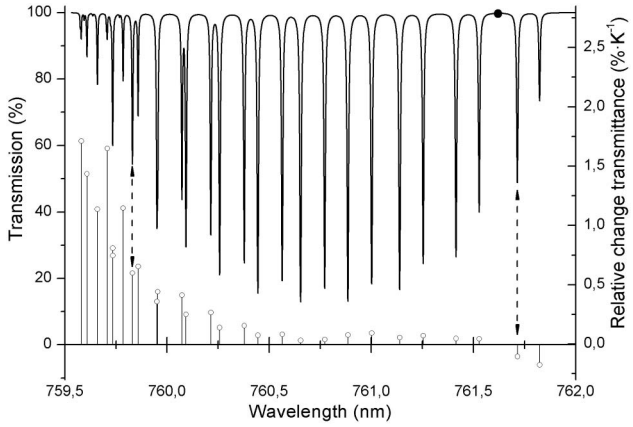

Fig. 2. Oxygen A-band transmission spectrum for a 67 m path in ambient air and the relative change in transmission for the strongest transitions [19]. The transitions used in this work are marked with dashed double arrows and the black dot marks the position of the baseline.

Oxygen concentration can be determined by sweeping the laser frequency over the whole absorption feature and fitting a Voigt profile to the measured absorption. The integrated line area can be calculated from the fit parameters to determine the concentration. Thermometry using the whole absorption feature is relatively straightforward, since broadening effects do not affect the normalized line shape function. Unfortunately, we were unable to achieve low uncertainty using fitting to the whole absorption profile in our very early tests. We aimed at real-time analysis and used a simple Lorentzian profile, which explains the problems we had in the fitting procedure. Therefore, we chose another method in which the peak absorption and baseline are measured. This method proved to be rapid and robust even in an outdoor environment. However, when measuring only the absorption peak, temperature and pressure affect the relative contributions of the Gaussian and Lorentzian components in the Voigt line shape, which changes the peak value of the line shape function. The effect of collisional, or Dicke, narrowing was investigated using a Galatry profile in the calculations [30,31]. The effect was found insignificant when compared to the result obtained using the convoluted Voigt profile.

The Doppler-broadened half-width, which is characterized by a Gaussian profile, depends on the wavelength, temperature, and mass of the molecule.

Increased temperature will increase the Doppler half-width and decrease the observed line width depending on the temperature coefficient n of the transition according to the empiric equation $\gamma_{\mathrm{air}}(T) = \gamma_{\mathrm{air}}(T_0) \times (T_0/T)^n$. This will result into a higher peak value of the absorption profile as the Gaussian line profile component becomes more dominant. Since the air broadened half-widths and the temperature coefficients are different for the two oxygen transitions, the temperature will have an effect on the line intensity ratio. For example, for a temperature change of −10 K (296 K → 286 K), the temperature determined from the ratio of the transmission minimums of transition 1 and transition 2 will be 76 mK higher if the temperature dependence of the line profile is taken into account, compared to the situation where this dependency is omitted. One should note that even small errors in, e.g., the temperature coefficient n can have a major impact on the final results. By using a temperature coefficient of 0.71 for both transitions, the same −10 K temperature change would result in a 233 mK lower temperature. This correction is important especially when measuring very high temperature variations. It affects systems based on the WMAS technique as well.

Varying pressure affects the observed total linewidth in a similar manner as the varying temperature. An increase in the pressure increases the width of the Lorentzian component and decreases the relative contribution of the Gaussian component. As an example, if the pressure is decreased by 1 kPa (101.3 kPa → 100.3 kPa), a 58 mK correction term must be added to the temperature determined by Eq. (4). In this work, a pressure correction factor α_{pres}, which is accurate for typical pressure variations in the ambient air, was used to correct the ratio R according to

$$R\left(1+\alpha_{\mathrm{press}}\left(\frac{p-p_{\mathrm{ref}}}{p_{\mathrm{ref}}}\right)\right) = R_0 \exp\left[-\frac{hc\Delta E}{k}\left(\frac{1}{T}-\frac{1}{T_{\mathrm{ref}}}\right)\right], \tag{5}$$

where p_{ref} is the reference pressure (101.3 kPa). The temperature of the air can be directly calculated according to

$$T(R,p) = \frac{T_{\mathrm{ref}}}{1-\frac{T_{\mathrm{ref}}k}{hc\Delta E}\ln\left(\frac{R}{R_0}\left(1+\alpha_{\mathrm{press}}\left(\frac{p-p_{\mathrm{ref}}}{p_{\mathrm{ref}}}\right)\right)\right)}. \tag{6}$$

4. Obtaining the Parameters of the Model

The parameters for the model presented by Eq. (6), which are given in Table 3, had to be obtained from experimental data mainly for two reasons. First, the values in the HITRAN database are not accurate enough for high-resolution thermometry. The database values for the uncertainty of the line intensity and linewidth are between 1% and 2% for transitions 1 and 2, while the uncertainty in the line intensity ratio should be of the order of 10^{-4} in order to obtain the temperature with ∼12 mK uncertainty. Second, the wavelength-dependent losses in any of the optical components after the power normalization affect the results. A known source of a systematic error is the wavelength-dependent reflectivity of the dielectric mirror (Thorlabs BB2-E03) that was used as the end mirror in the measurement path. Because the wavelength dependency of the system was not explicitly characterized, the obtained parameters given in Table 3 are valid only for the presented temperature measurement configuration.

Table 3. Parameters Required for the Presented Spectroscopic Two-Line Thermometry

Data Source	ΔE (cm^{-1})	R_0 (1)	α_{pres} (1)
Database[a]	−542.4	1.1385	0.0500
Fit	−520.0	1.1571	0.0506

[a]HITRAN values are from the 2008 database.

The measurement procedure is similar to that in our previous work [19]. A typical measurement of oxygen transmission is shown in Fig. 3. It was done outdoors over a 130 m path. One-hundred data points were collected for both features. Transition 2 is left out of Fig. 3 for clarity. In the measurements performed in the laboratory environment, the final baseline value is simply the average of all the measurement points. In the measurements done outdoors, we removed all data points that were at least 3 times the standard deviation off the average. We subsequently obtained the baseline by calculating the average of the corrected data. The erroneous data points were not common, which led to the conclusion that they were most likely caused by falling leaves and flying insects that occasionally blocked the laser beam during the measurements, which were done in October. A second-order polynomial fit to the measured transmission data is shown in Fig. 3. It was used in the outdoor measurements

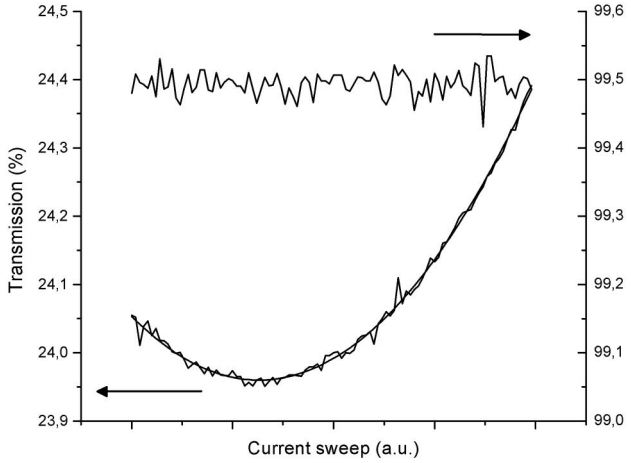

Fig. 3. Typical oxygen transmission measurement of transition 1 and baseline over a 130 m path measured outdoors including a second-order polynomial fit, which is used to determine the absorption peak.

due to the random erroneous data points. A simple 15-point moving average was used in the indoor measurements, in which case it was found to be the best method to determine the minimum transmission. The laser frequencies were loosely stabilized to the absorption line centers using data of the previous measurement and a relatively wide sweep area had to be used to ensure that the transmission minimum would be always found.

The small absorbance due to the tails of the Voigt profile causes the transmission to drop by approximately 0.5% at the point of the baseline measurement shown in Fig. 3. The intensity of an individual line is then calculated using Eq. (1) from the corrected baseline value and from the value of the minimum transmission. The same baseline is used to calculate the line intensity of both transitions. The air temperature is calculated using Eq. (6), which takes into account the pressure correction term. The temperature correction term, which is not explicitly shown in Eq. (6), is added to the temperature given by Eq. (6) to obtain the final temperature value.

The standard deviations of the baseline and the transition 1 measurement shown in Fig. 3 were 1.83×10^{-4} and 0.82×10^{-4}, respectively. The standard deviation of the sample mean is a factor of 10 lower for the baseline because the whole 100-point sample is used for averaging. In the temperature measurements done indoors, the standard deviation of the sample mean is approximately 4 times lower, because of the 15-point moving average. In the measurement shown in Fig. 3, we estimate that the standard deviation of the sample mean is approximately by a factor of 10 lower, because the fit to the second-order polynomial is good. These values for the standard deviations of the spectroscopic data indicate that the standard deviation of the temperature should be of the order of 3 mK according to Eq. (6) when using a value of 1.3×10^{-5} as the standard deviation of the sample mean for both transitions and for the baseline.

Experiments were done in a temperature- and humidity-controlled laboratory above a 30 m long interferometric measurement rail used for length metrology. Eight calibrated Pt-100 sensors were spaced evenly across the measurement path and their average was used as the reference temperature. Pt-100 sensors were positioned in close proximity of the beam path to ensure good lateral spatial overlap. The sensor closest to the measurement head was at slightly higher temperature than the others, due to heat generated by the electronics of the measurement head. The temperature controller of the laboratory room acts by adjusting the temperature of the incoming air. Temperature variations were induced by adjusting the set point of the controller. The result of a typical 62 h measurement is shown in Fig. 4. The period from 48 to 62 h was used to calculate the noise of the measurement. The RMS noise was 7 mK using a sample a time of 120 s. The black line represents the average of the reference sensors and the gray line shows the fit based on Eq. (6).

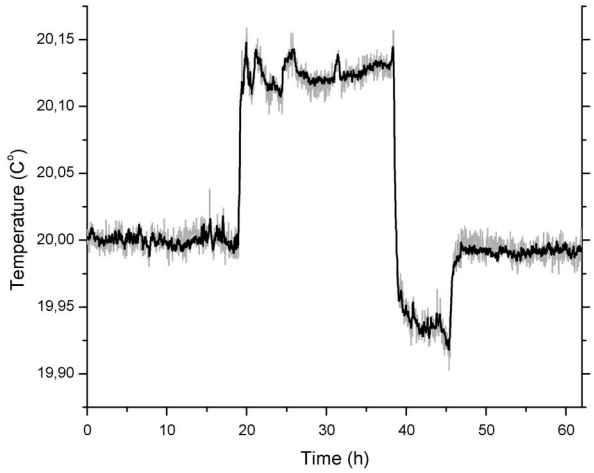

Fig. 4. Parameter calibration results of the spectroscopic thermometer measurement (gray) fitted to the ensemble of Pt-100 sensors (black) spaced evenly over the 67 m path length. The temperature variations were done by adjusting the temperature of the incoming air.

Since the temperature measurement is done in open laboratory space, the 7 mK RMS noise, which is larger than the 3 mK RMS estimate based on the transmission measurements, also includes the fluctuations in the air temperature and drifts in the mechanics and electronics. The RMS noise of the ensemble of Pt-100 sensors was 2.5 mK during the same measurement period. However, due to the relatively long time constant of the Pt-100 sensors, part of the rapid fluctuations in the air temperature are low-pass filtered, which likely explains the difference.

The temperature controller of the laboratory operates in a narrow set-point range and we were not able to induce large temperature variations. For such a narrow temperature range, the temperature effects described in Section 3 are insignificant. The pressure varied between 100 and 101.2 kPa during the measurement. The parameters obtained from the fit and the values calculated using the database are given in Table 3. The rotational energy difference and the ratio R_0 of the two absorption lines at the reference temperature and pressure are fairly close to values given in the HITRAN database. The pressure correction factor is in good agreement with the database value. If the database values for rotational energy difference and for the ratio at a reference temperature T_0 are used with the ratio R obtained from the fit, the spectroscopically determined temperature at standard pressure is 22.85 °C instead of the 21.05 °C obtained by using the fitted parameter values.

5. Measurements

To test the capability of the system to compensate the refractive index of air for an interferometric length measurement, we set up a heterodyne laser

interferometer (HP 5518) on top of the measurement rail. The path lengths of the interferometric system and the spectroscopic system were set to within a few centimeters of each other by fixing the corner cube of the interferometer to the measurement head of the spectroscopic measurement. Ideally, the beams should overlap to ensure the most effective compensation of the air refractive index, but for practical reasons the beams were not combined. The beams were at the same height and the separation of the beams was less than 10 cm over the whole measurement path. Two electric heaters and a fan, positioned close to the center of the measurement path and 2 m above the measurement rail, were used to induce rapid local air temperature variations. The heaters caused approximately 2.5 K local temperature rise, changing average temperature over the measurement path by 0.6 K. There was no significant increase in the temperature near the end mirror and the measurement head. The average temperature measured with the spectroscopic system (curve 4) and with the Pt-100 sensor ensemble (curve 3) are shown Fig. 5. A compensated interferometric reading is given in the upper part of Fig. 5 for both spectroscopic temperature measurement (curve 2) and the ensemble average of the Pt-100 sensors (curve 1). The temperature determined by the spectroscopic system was approximately 10 mK lower than the reference temperature between the heating periods. This could be caused by the realignment of the optics during the assembly of the interferometric system.

From the data it is clearly seen that the spectroscopic method compensates very well even local air temperature changes in interferometric displacement measurements. The heating periods are almost invisible in the interferometer measurement, except for some transients. On the other hand, one can see that even with eight Pt-100 sensors, evenly spaced over a 30 m beam path, it is not possible to reach a good compensation if there are significant temperature gradients. During the measurements, the ambient pressure varied between 99.1 and 100.4 kPa. The 120 s sample time of the spectroscopic system explains transients in compensated displacement when the heating is turned on and off rapidly. The ~5 μm long-term drift in the measured displacement is probably caused by a real mechanical displacement of the concrete beams where the interferometer setup was mounted.

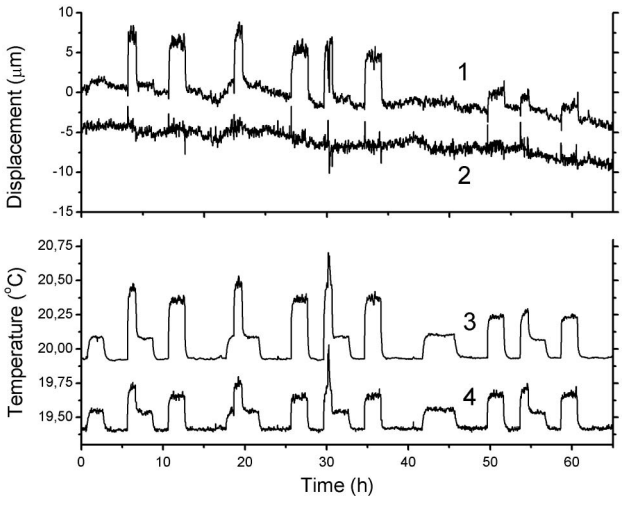

Fig. 5. Top, interferometric length compensated by using Pt-100 sensors (curve 1) and by using the spectroscopic temperature measurement (curve 2). Bottom, average temperatures along the path length with local temperature variations measured by the Pt-100 sensors (curve 3) and by the spectroscopic system (curve 4). For clarity, −5 μm and −500 mK offsets have been added to the spectroscopically compensated displacement (2) and to the spectroscopically determined temperature (4), respectively.

Outdoor measurements were conducted at the Nummela baseline of the Finnish Geodetic Institute. The measurement setup, except for the measurement head, was kept in a heated room with no active temperature control. The measurement head was positioned outdoors with no temperature control. The ambient temperature varied between 5 °C and 15 °C during a typical measurement day. The distance between the end mirror and the measurement head was 65 m, making the total measurement distance 130 m. Although the long path length causes decrease in sensitivity due to saturation in the transmission, we chose to use the same two transitions as shown in Fig. 2, because their properties were well characterized in the laboratory. Ten Pt-100 sensors were used as a reference with approximately equidistant spacing and close proximity to the laser beam. The spectroscopically measured temperature and the average of the Pt-100 sensors are shown in Fig. 6. The gray line represents the spectroscopic temperature, which is approximately 200 mK lower than the reference temperature given by the Pt-100 sensors for the last 6 h. Sun was shining for the first 2 h, which could explain the difference in the offset in

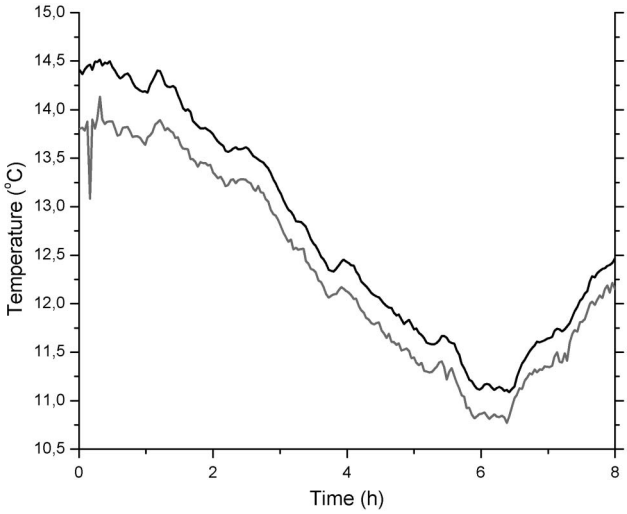

Fig. 6. Average temperature measured at Nummela baseline over a 130 m path length. Average of Pt-100 sensors is marked by black curve. Gray curve represents the spectroscopically measured temperature.

the beginning. The Pt-100 sensors were not protected from direct sunlight.

After the outdoor measurements, we transported the setup back to the laboratory and tested it in a temperature-controlled laboratory room to verify a broader temperature range. A good fit was found between the reference Pt-100 sensors and the spectroscopic method for a temperature range of 16 °C to 25 °C. The parameters of the previous fit could not be used, as we had to use several wavelength-dependent mirrors in order to achieve a path length of 40 m in a small laboratory room. Although we used only a limited temperature range to fit the parameters of Eq. (6), the model was found to be accurate also over a broader temperature range. Therefore, we expect that the temperature offset observed in the outdoor measurements is predominantly affected by the transportation of the setup compared to the uncertainty in the transition parameters discussed in Section 2. For example, the beam splitter had slightly moved during the transportation, which was observed only later. The 200 mK offset corresponds to approximately 1.7×10^{-3} difference in the line intensity ratio. Part of the difference could be also explained by nonideal collimation of the laser beams, which we could not verify in the outdoor environment.

6. Discussion and Conclusions

A spectroscopic method for on-line compensation of air refractive index over longer distances has been described and demonstrated experimentally. The method is capable of measuring average air temperature along approximately the same beam path that is used for optical length measurement. The method provides potentially excellent spatial and temporal overlap and, therefore, accurate air temperature compensation. A drawback of the present setup is the modest time resolution, approximately 120 s. The main reason for the limited time resolution is that just one laser is used to probe the absorption peak and the baseline, which means that the laser wavelength has to be repeatedly tuned between the two wavelengths. The wavelength tuning is done by laser temperature, causing 30 s dead time after each adjustment using our equipment. Another disadvantage of the present setup is the lack of active wavelength stabilization. For this reason, the wavelength scan over an absorption line has to be rather wide to ensure that the peak absorption is captured during each scan. Therefore, the total number of measured points is much larger than what is actually needed for the final analysis. The measurement speed could be significantly improved if a method to stabilize the laser frequency to the absorption peak would be developed. This could be achieved, for example, by using a third-harmonic locking scheme and an external low-pressure oxygen cell or a hollow fiber filled with oxygen. One possibility would be to use the second-harmonic signal at the locked wavelength of the absorption maximum to determine the temperature [11–14]. In this way, there would not be any wasted data points and the time resolution would be determined by the shutter switching time and the lock-in amplifier settling time. We estimate that a time resolution of a few seconds could be possible to achieve without increasing the measurement noise considerably.

We have demonstrated, to our knowledge, the most precise spectroscopic temperature measurement of air. Our system allows measurements over long distances of up to 130 m with a RMS noise of 7 mK for a 120 s averaging time, which corresponds to $\sim 0.7 \times 10^{-8}$ RMS noise in the refractive index of air. The obtained noise level is considerably lower than the 22 mK RMS noise using the 60 s averaging time presented in our previous work [19].

The accuracy of the temperature measurement system is difficult to evaluate. Re-evaluation of the data presented in our earlier study [19] showed a 20 mK offset when changes were made to the system during the measurement. Considering the 10 mK offset that was observed in our current temperature measurement system during the interferometric tests, we believe that, with the current system and calibration, we are able to determine the air temperature with accuracy high enough to safely reach an uncertainty smaller than 10^{-7} in the refractive index of air from a 16 °C to 25 °C temperature range in a laboratory environment.

Compensation of the refractive index of air required for high-accuracy length measurements has been shown to be feasible even when significant local temperature variations are induced. The effect of the line profile composition and the sensitivity of the method to transition parameters have been discussed. Outdoor measurement results are in agreement with the laboratory experiments except for an offset, which can be explained by major alignment changes caused by the transportation and possibly nonideal collimation of the laser beams.

Research within the European Association of National Metrology Institutes (EURAMET) joint research project leading to these results has received funding from the European Community's Seventh Framework Programme, ERA-NET Plus, under Grant Agreement No. 217257. The authors thank Dr. J. Jokela from the Finnish Geodetic Institute for his help during the Nummela measurements.

References

1. K. P. Birch and M. J. Downs, "The results of a comparison between calculated and measured values of the refractive index of air," J. Phys. E **21**, 694–695 (1988).
2. G. Bonsch and E. Potulski, "Measurement of the refractive index of air and comparison with modified Edlén's formulae," Metrologia **35**, 133–139 (1998).
3. B. Edlen, "The refractive index of air," Metrologia **2**, 71–80 (1966).
4. P. E. Ciddor, "Refractive index of air: new equations for the visible and near infrared," Appl. Opt. **35**, 1566–1573 (1996).
5. A. Lassila, "Updated performance and uncertainty budget of MIKES' line scale interferometer," in *Proceedings of 4th*

EUSPEN International Conference (EUSPEN, 2004). pp. 258–259.
6. A. Lassila, M. Kari, H. Koivula, U. Koivula, J. Kortstrom, E. Leinonen, J. Manninen, J. Manssila, T. Mansten, T. Merilainen, J. Muttilainen, J. Nissila, R. Nyblom, K. Riski, J. Sarilo, and H. Isotalo, "Design and performance of an advanced metrology building for MIKES," Measurement **44**, 399–425 (2011).
7. V. Korpelainen and A. Lassila, "Acoustic method for determination of the effective temperature and refractive index of air in accurate length interferometry," Opt. Eng. **43**, 2400–2409 (2004).
8. A. Y. Chang, M. D. DiRosa, D. F. Davidson, and R. K. Hanson, "Rapid tuning cw laser technique for measurements of gas velocity, temperature, pressure, density, and mass flux using NO," Appl. Opt. **30**, 3011–3022 (1991).
9. M. P. Arroyo and R. K. Hanson, "Absorption measurements of water-vapor concentration, temperature, and line-shape parameters using a tunable InGaAsP diode laser," Appl. Opt. **32**, 6104–6116 (1993).
10. D. S. Baer, R. K. Hanson, M. E. Newfield, and N. K. J. M. Gopaul, "Multiplexed diode-laser sensor system for simultaneous H_2O, O_2, and temperature measurements," Opt. Lett. **19**, 1900–1902 (1994).
11. J. Silver and D. J. Kane, "Diode laser measurements of concentration and temperature in microgravity combustion," Meas. Sci. Technol. **10**, 845–852 (1999).
12. J. T. C. Liu, J. B. Jeffries, and R. K. Hanson, "Large-modulation-depth 2*f* spectroscopy with diode lasers for rapid temperature and species measurements in gases with blended and broadened spectra," Appl. Opt. **43**, 6500–6509 (2004).
13. X. Zhou, J. B. Jeffries, and R. K. Hanson, "Development of a fast temperature sensor for combustion gases using a single tunable diode laser," Appl. Phys. B **81**, 711–722 (2005).
14. J. Shao, L. Lathdavong, P. Kluczynski, S. Lundqvist, and O. Axner, "Methodology for temperature measurements in water vapor using wavelength-modulation tunable diode laser absorption spectrometry in the telecom C-band," Appl. Phys. B **97**, 727–748 (2009).
15. M. G. Allen, "Diode laser absorption sensors for gas-dynamic and combustion flows," Meas. Sci. Technol. **9**, 545–562 (1998).
16. V. Ebert, T. Fernholz, C. Giesemann, H. Pitz, H. Teichert, J. Wolfrum, and H. Jaritz, "Simultaneous diode-laser-based *in situ* detection of multiple species and temperature in a gas-fired power plant," Proc. Combust. Inst. **28**, 423–430 (2000).
17. S. T. Sanders, J. Wang, J. B. Jeffries, and R. K. Hanson, "Diode-laser absorption sensor for line-of-sight gas temperature distributions," Appl. Opt. **40**, 4404–4415 (2001).
18. H. Teichert, T. Fernholz, and V. Ebert, "Simultaneous *in situ* measurement of CO, H_2O, and gas temperatures in a full-sized coal-fired power plant by near-infrared diode lasers," Appl. Opt. **42**, 2043–2051 (2003).
19. T. Hieta and M. Merimaa, "Spectroscopic measurement of air temperature," Int. J. Thermophys. **31**, 1710–1718 (2010).
20. V. Spagnolo, L. Dong, A. A. Kosterev, D. Thomazy, J. H. Doty III, and F. K. Tittel, "Modulation cancellation method for measurements of small temperature differences in a gas," Opt. Lett. **36**, 460–462 (2011).
21. F. Pollinger, T. Hieta, M. Vainio, N. R. Doloca, A. Abou-Zeid, K. Meiners-Hagen, and M. Merimaa, "Effective humidity in length measurements: comparison of three approaches," Meas. Sci. Technol. (to be published).
22. Further information on HITRAN available from www.hitran.com.
23. D. J. Robichaud, J. T. Hodges, P. Maslowski, L. Y. Yeung, M. Okumura, C. E. Miller, and L. R. Brown, "High-accuracy transition frequencies for the O_2 *A*-band," J. Mol. Spectrosc. **251**, 27–37 (2008).
24. D. J. Robichaud, J. T. Hodges, L. R. Brown, D. Lisak, P. Maslowski, L. Y. Yeung, M. Okumura, and C. E. Miller, "Experimental intensity and lineshape parameters of the oxygen *A*-band using frequency-stabilized cavity ring-down spectroscopy," J. Mol. Spectrosc. **248**, 1–13 (2008).
25. L. R. Brown and C. Plymate, "Experimental line parameters of the oxygen *A* band at 760 nm," J. Mol. Spectrosc. **199**, 166–179 (2000).
26. Y. Liu, J. Lin, G. Huang, Y. Guo, and C. Duan, "Simple empirical analytical approximation to the Voigt profile," J. Opt. Soc. Am. B **18**, 666–672 (2001).
27. Q. V. Nguyen, R. W. Dibble, and T. Day, "High-resolution oxygen absorption spectrum obtained with an external-cavity continuously tunable diode laser," Opt. Lett. **19**, 2134–2136 (1994).
28. V. G. Avetisov and P. Kauranen, "High-resolution absorption measurements by use of two-tone frequency-modulation spectroscopy with diode lasers," Appl. Opt. **36**, 4043–4054 (1997).
29. P. Vogel and V. Ebert, "Near shot noise detection of oxygen in the A-band with vertical-cavity surface-emitting lasers," Appl. Phys. B **72**, 127–135 (2001).
30. L. Galatry, "Simultaneous effect of Doppler and foreign gas broadening on spectral lines," Phys. Rev. **122**, 1218–1223 (1961).
31. P. L. Varghese and R. K. Hanson, "Collisional narrowing effects on spectral line shapes measured at high resolution," Appl. Opt. **23**, 2376–2385 (1984).